Applied Catalysis B: Environmental 187 (2016) 67–74

Contents lists available at ScienceDirect

Applied Catalysis B: Environmental

journal homepage: www.elsevier.com/locate/apcatb

Highly efficient graphene oxide/porphyrin photocatalysts for hydrogen evolution and the interfacial electron transfer

Riyue Ge [a], Xiangqing Li [a,*], Shi-Zhao Kang [a], Lixia Qin [a], Guodong Li [b]

[a] School of Chemical and Environmental Engineering, Center of Graphene Research, Shanghai Institute of Technology, 100 Haiquan Road, Shanghai 201418, China

[b] State Key Laboratory of Inorganic Synthesis and Preparative Chemistry, College of Chemistry, Jilin University, Changchun 130012, China

ARTICLE INFO

Article history:
Received 1 September 2015
Received in revised form
24 December 2015
Accepted 10 January 2016
Available online 15 January 2016

Keywords:
Graphene oxide
Porphyrin
Interfacial linkers
Photocatalysis
Hydrogen energy

ABSTRACT

By implanting metal ions as interfacial linkers of the graphene oxide (GO) and 5,15–diphenyl–10,20–di(4–pyridyl)porphyrin (DPyP), a serial of novel GO–DPyP nanocomposites were achieved. In these composites, GO and DPyP were bridged by the metal ions by means of electrostatic interaction and coordination interaction. It was shown that the metal ions can modify the morphology and structure of the GO–DPyP nanocomposite, and facilitate electron transfer between GO and DPyP. Furthermore, the photocatalytic hydrogen evolution activity and electron transfer mechanism were investigated. The results demonstrated that the strong interaction and efficient electron transfer between the metal ions and DPyP/GO were the important reasons for the improvement of the photocatalytic hydrogen evolution performance. Implanting metal ions in the interface of graphene oxide and porphyrin is a simple and efficient approach to optimize the transfer pathway of photogenerated electrons and improve catalytic performance of nanocomposites.

1. Introduction

Due to the shortage of fossil fuels and environmental pollution, it is important to develop a new kind of energy. Hydrogen, as an exciting renewable and clean source, has been studied for many years. It is found that using solar energy to produce clean hydrogen through photocatalysis is a good choice [1]. However, the conversion efficiency of the current materials is still low due to weak light absorption ability, rapid recombination of electron–hole and low stability. It is the key to design and synthesize ideal catalysts for photocatalytic hydrogen evolution.

Graphene oxide (GO) possesses the excellent characteristics of graphene, such as large specific surface area, highly electronic and thermal conductivity [2]. In addition, the abundant functional groups, such as epoxide, hydroxyl and carboxyl groups, make GO easily be further modified. It is reported that GO can be functionalized with some photosensitive materials through the covalent or noncovalent interaction [3–7]. Subsequently, the electron transfer from excited photosensitive molecules to GO sheets can take place, which has been considered to be important means to improve photocatalytic properties of the graphene–based photocatalysts.

Porphyrin has been used in catalytic field because of its special structure and high thermal stability [8,9]. Porphyrin/carbon–based functional materials, such as porphyrin/carbon nanotubes and porphyrin/graphene sheets linked by covalently or non–covalently approaches have been one of the hottest candidates [10–14]. While improving electron transfer efficiency between graphene and porphyrin is an efficient way to enhance the photocatalytic activity of the graphene/porphyrin composites. The porphyrin/graphene composites linked by covalent bond show high electron transfer efficiency due to low interface resistance [11]. However, the complicated process and low yield are obstructions in practical application. How to improve the electron transfer between porphyrin and graphene by a facial method is an important topic in this field.

It is reported that multistep electron transfer via ZnO nanoparticles mediator linking graphene and porphyrin exhibits remarkably high photocurrent generation [12]. In addition, the graphene–based photocatalysts prepared by inorganic or organic modification on graphene sheets show enhanced catalytic activity [15,16]. It was found that, employing polyaniline as the coupling linker, the controlled growth of MO/MH (such as Co_3O_4, Fe_2O_3, and $(Ni(OH)_2)$NPs) on graphene was achieved, and the conductivity of MO/MH and the coupling effects between graphene and MO/MH were improved [17]. Using glucose as the linker and face–controlling agent, Zhang et al. prepared the

* Corresponding author.
E-mail address: xqli@sit.edu.cn (X. Li).

http://dx.doi.org/10.1016/j.apcatb.2016.01.024
0926-3373/

TiO_2 with the (001) facets and a mesoporous structure [18]. Employing 2D GO/SnO_2 nanosheets as the basic building block and various amphiphilic polymers including poly(vinyl alcohol), Pluronic®F127, polyethylenimine and GO as the cross–linkers, macroporous graphene/SnO_2 frameworks with tunable macroporosity (2 to 50 μm) have been achieved [19]. Xu et al. prepared a GO/CdS nanoparticles with metal ions as the linker, which shows high photocatalytic activity in selective oxidation of benzyl alcohol and selective reduction of 4–nitroaniline [20]. Yu et al. prepared graphene oxide (GO)/polyacrylamide (PAM) hydrogels by the synergistic effects of GO and calcium ions. The role of the Ca^{2+} is mainly to induce dissipation of the on–loading crack energy of GO network, and contribute to the higher stretch ability [21]. It is known that the coordination of metal ions with nitrogen–based ligands is an important interaction [22]. Kira et al. found that pyridylfullerene (Py–C_{60}) acceptors can infiltrate into the metalloporphyrin zinc brush by the coordination of the pyridyl moiety to the zinc atom together with π–π interaction between the Py–C_{60} moieties, which efficiently improves the performance of organic photovoltaic [23]. Due to its smaller radius, the metal ions as the interfacial linkers could be more profitable to decrease the interfacial resistance between GO and DPyP and to improve the transfer efficiency of photoproduced electrons.

In this paper, with various metal ions as the interfacial linker, (5,15-diphenyl)-10,20-di(4-pyridyl) porphyrin as light absorbing antenna, and graphene oxide as the electron transfer support, by coordination interaction and electrostatic interaction, a serials of graphene oxide/porphyrin donor–acceptor nanocomposites (GO–DPyP) are constructed at room temperature by a simple and environmentally friendly approach. The influence of metal ions on the morphology and structure of the nanocomposites, photocatalytic activity and electron transfer mechanism for the composites are studied.

2. Experimental

2.1. Materials

5,15–diphenyl–10,20–di(4–pyridyl) porphyrin (DPyP) was purchased from J&K Scientific Ltd. Graphite powder with an average size of 30 μm and purity of >99.85% was purchased from Shanghai Chemical Reagent Company. All the other chemical reagents (A.R.) were purchased from Sinopharm Chemical Reagent Co. and were used without further purification. Double distilled water was used throughout the experiments.

2.2. Preparation of GO

GO was prepared by a modified Hummers method [24,25]. In brief, commercially available graphite powder (1 g) was mixed with $NaNO_3$ (1 g) and H_2SO_4 (80 mL) and sonicated in an ice bath for 30 min. Subsequently, $KMnO_4$ (8.5 g) was added in small portions to the mixture, and continually sonicated for 15 min. Then the mixture was stirred for 1 h at 40 °C. Double distilled water (50 mL) was slowly added and stirred for another 1.5 h. The suspension was kept at 90 °C for 1 h. After adding H_2O_2 (45 mL, 30 vol.%) and HCl (500 mL, 10 vol.%), respectively, the mixture was aged for 24 h. The brown precipitate (GO) obtained by centrifuging was washed until the pH of the filtrate was about 7. Finally, the solid was dried overnight at 60 °C.

2.3. Preparation of GO–M–DPyP composite

The simple strategy used to prepare the GO–M–DPyP composites is depicted in Scheme 1. In a typical procedure, a certain amount of the salt solution (M = K^+, Ca^{2+}, Zn^{2+}, Cu^{2+}, Co^{2+} or Cr^{3+}) was added to 200 mL of 0.5 mg mL^{-1} GO aqueous dispersion solution. Next, the above mixture was stirred for 2 h at room temperature. Then, the mixture was centrifuged and washed for several times with double distilled water. Finally, the solid obtained (GO–M) was dried overnight at 60 °C. The implanted content of metal ions was about 10%.

DPyP tetrahydrofuran (THF) solution (5 mL, 1 mmol L^{-1}) was injected into GO–M aqueous dispersion (155 mL, 0.5 mg mL^{-1}) under vigorous stirring, and stirred for 2 h at room temperature. Afterwards, the GO–M–DPyP composite was achieved by centrifuged and dried at 45 °C. By replacing the GO–M with the GO, the GO–DPyP composite was prepared in the same procedure as that of the GO–M–DPyP composite. The content of DPyP in the composites was about 4 wt.%.

2.4. Characterizations

UV–vis absorption spectra were recorded with a UV–3900 spectrophotometer (Japan). Fourier transform infrared spectra (FTIR) were recorded on a Nicolet 6700 FTIR spectrometer (USA). Transmission electron microscope (TEM) images were taken with a JEOL JEM–2100F microscope device (Japan), and the accelerating voltage was 200 kV. The morphology of the composite was observed by S–3400 N Hitachi High Technologies scanning electronic microscopy (SEM, Japan). The element maps were taken with FEI Tecnai G^2 20 high resolution transmission electron microscope (USA). Nitrogen adsorption–desorption isotherm was obtained at 77 K by using Micrometrics Model ASAP 2020 volumetric adsorption analyzer (USA). The sample was pre-outgassed at 333 K under vacuum. X – ray photoelectron spectra (XPS) were measured on a Thermo ESCALAB 250 X–RAY photo electron spectrometer with a monochromatic X–ray source (Al Kα $h\nu$ = 1486.6 eV) (USA). X – ray powder diffraction (XRD) was carried out using a Bruker D8 Advance X–ray diffractometer (Germany). The thermo–gravimetric/differential thermal analyzer (TG – DTA) was recorded on a Mettler–Toledo TG/DTA instrument under N_2 atmosphere (Switzerland). The heating rate was 10 °C min^{-1}.

Scheme 1. The synthesis procedure for the GO–M–DPyP composite.

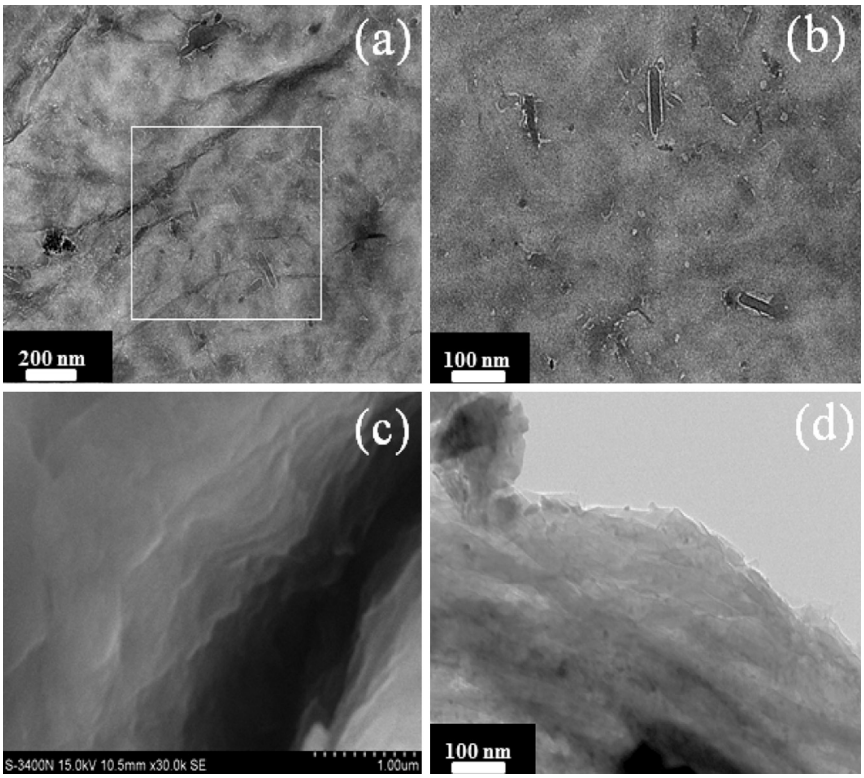

Fig. 1. TEM images for the GO–DPyP nanocomposite (a and b); SEM (c) and TEM (d) images for the GO—Cr^{3+}–DPyP composite.

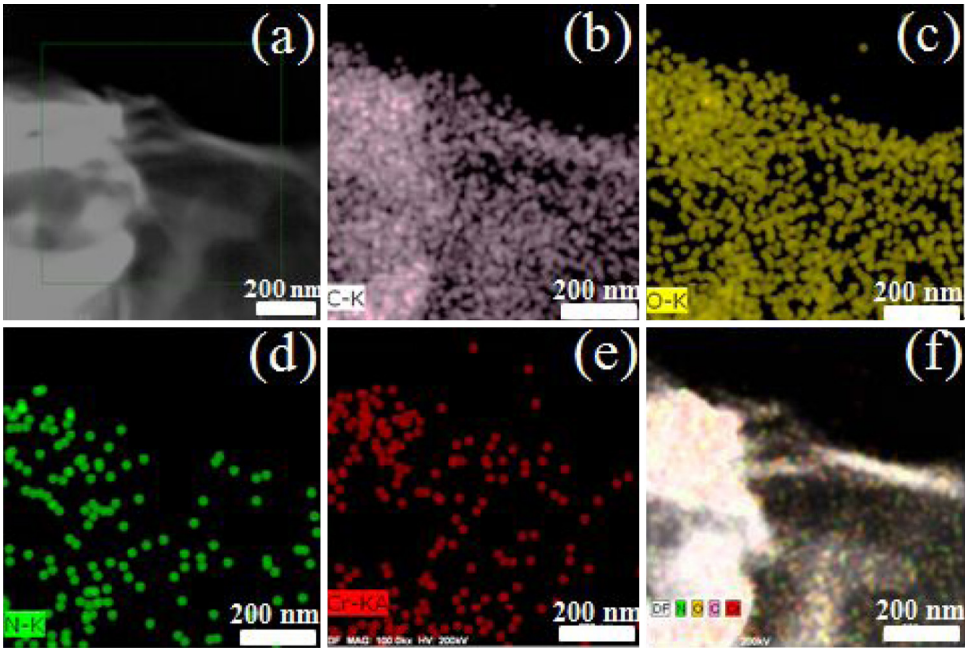

Fig. 2. Energy–filtered TEM image of the GO—Cr^{3+}–DPyP composite (a). Element maps: (b) C map; (c) O map; (d) N map; (e) Cr map and (f) zero–loss map of C, N, O and Cr elements, respectively.

2.5. Photoelectrochemical measurements

First, fluorine–doped tin oxide (FTO) glasses were cleaned by sonication in ethanol, acetone, chloroform and double distilled water for 15 min, respectively, and then dried in the atmosphere. FTO glasses coated with the sample were used as working electrodes, which were prepared via impregnation and subsequent calcination. In brief, 10 mg of sample (GO – DPyP or GO – M – DPyP) was added into 2 mL of alcohol, and the mixture was sonicated for 30 s. After that, the FTO glass ($1 \times 1.5\ cm^2$) was soaked into the slurries for 1 min, and heat – treated at 60 °C for 1 h.

The photoelectrochemical and EIS measurements were carried out at room temperature using Chenhua CHI 660E computer – controlled electrochemical analyzer with a standard three – electrode system. Ag/AgCl electrode was used as the

reference electrode, and a platinum wire electrode was used as the counter electrode. The electrolyte was Na_2SO_4 aqueous solution.

Electrochemical impedance spectra (EIS) were measured in the potentiostatic mode with the frequency range of 0.01 Hz to 10^5 Hz, and the bias potential was 10 mV. The amplitude was 50 mV. The light source was a 300 W Xe lamp. The distance between light source and the working electrode was 7 cm. The air in the solution was removed by purging nitrogen for 15 min. The measurement was carried out in 0.01 mol L^{-1} $K_3Fe(CN)_6/K_4Fe(CN)_6$ (1:1) aqueous solution containing 0.1 mol L^{-1} KCl.

2.6. Measurement of photocatalytic activity

The photocatalytic hydrogen evolution over the samples was performed through a CEL–SP2 N water splitting system with a 300 W Xe lamp as the light source. In detail, 10 mg of the sample was dispersed into 60 mL of 10 vol.% triethanolamine aqueous solution. The reaction temperature was kept at about 25 °C by circulating water jacket. Before irradiation, it was evacuated by a vacuum pump in order to remove the air in the system. The amount of hydrogen evolution was analyzed by a continuous online gas chromatography (AULTT Co., Beijing) equipped with a thermal conductivity detector (TCD), and the high–purity N_2 (99.999%) was used as a carrier gas.

3. Results and discussion

3.1. Morphology and composition of the composites

The morphologies of the GO–DPyP and the GO–M(Cr^{3+})–DPyP composites are shown in Fig. 1. It can be seen that, without introducing metal ions, some short nanorods with 100–150 nm length can be observed on the sheet of the GO (Fig. 1a and b). Due to weak π–π interaction between GO and DPyP, the DPyP molecules only flattened onto the surface of the GO in the form of J–aggregates [26],

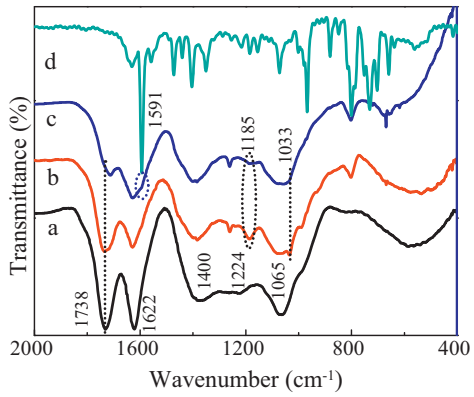

Fig. 3. FTIR spectra of GO (a); GO–DPyP composite (b); GO—Cr^{3+}–DPyP composite (c) and DPyP (d).

which prohibited the overlay of GO sheets. Differently, a layered nanostructure is formed after introducing Cr^{3+} ions between the GO and the DPyP. Moreover, thickness of the composite increases after introducing metal ions. Based on the morphological difference between GO–DPyP and GO–M–DPyP, it is deduced that metal ions anchored on the surface of GO can coordinate with two pyridyl moieties in the 5,15–diphenyl–10,20–di(4–pyridyl) porphyrin (DPyP), and the DPyP pillared GO composite is formed with the metal ions as the interfacial linker. The presence of the metal ions in the composite can be further proved from the following results (Fig. 2, Fig. 4, Fig. 6, Fig. 8 and Fig. 9).

Just like the experimental procedure demonstrated in Section 2.3 (Preparation of GO–M–DPyP composite): after a certain amount of salt solution reacted with GO aqueous dispersion solution for 2 h, GO–M composite was prepared via electrostatic attraction. The reaction between GO–M was hardly happened because of the electron repulsion (The large quantity loading of metal ions will greatly

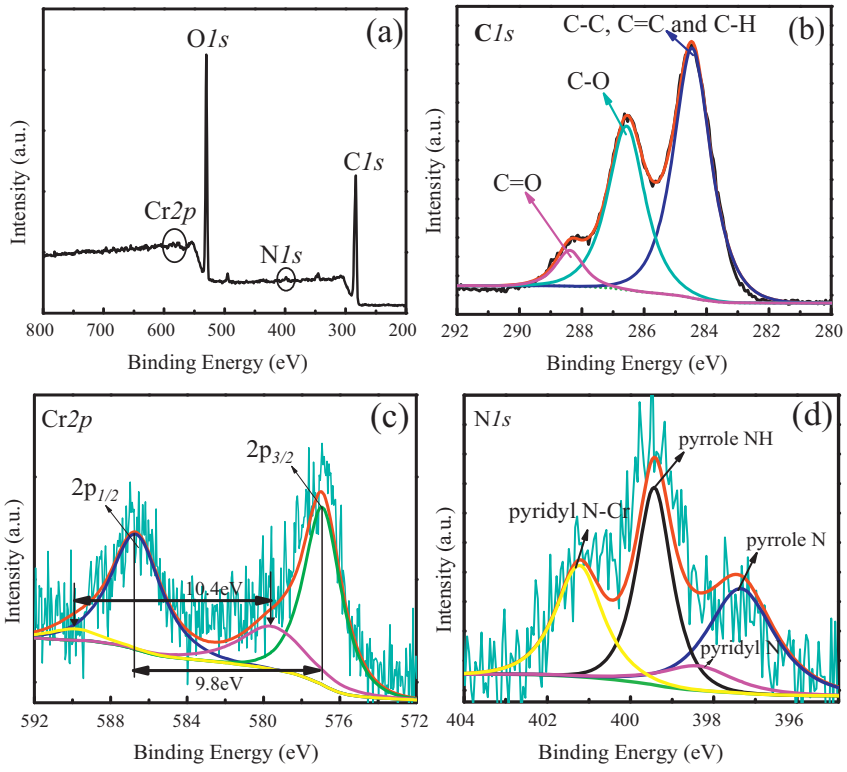

Fig. 4. XPS survey spectrum of GO—Cr^{3+}–DPyP composite (a); and the high–resolution spectra of C1s (b), Cr2p (c) and N1s (d).

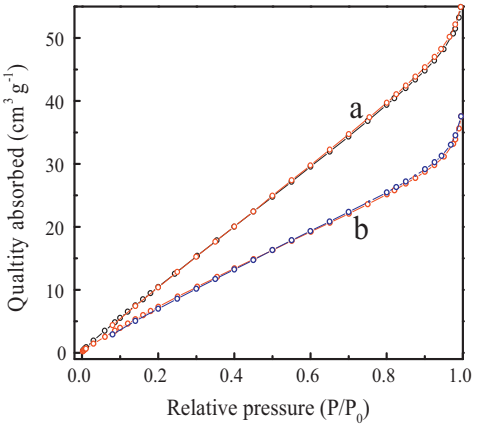

Fig. 5. Nitrogen adsorption–desorption isotherm of GO–DPyP composite (a) and GO—Cr^{3+}–DPyP composite (b).

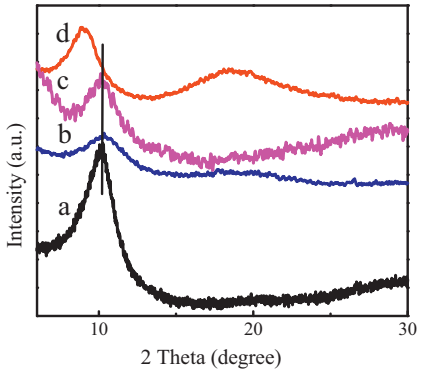

Fig. 6. XRD patterns of GO (a), GO–DPyP (b), GO – Cr^{3+} (c) and GO – Cr^{3+} – DPyP (d) composites.

weaken the interactions between the GO [27]). So the interfacial link will hardly exist between GO sheet and GO sheet.

In addition, GO–M composite was washed for several times with double distilled water in order to remove free metal ions and to restrain the link between DPyP and DPyP. In addition, the concentration of DPyP solution (3×10^{-5} mol L^{-1}) was low, self–aggregation among DPyP in the solution was almost ignored (Fig. S1).

Based on the result of TEM, the structural characteristics of DPyP and GO, and the above analysis, the formation process of the GO—Cr^{3+}–DPyP composite with the layered nanostructure could be illustrated in Scheme 2. Firstly, Cr^{3+} ions are absorbed onto the GO by electrostatic interaction; then, adding GO–M composite into the DPyP solution, the Cr^{3+} ions anchored on the surface of GO can coordinate with one pyridyl moiety in the 5,15–diphenyl–10,20–di(4–pyridyl) porphyrin (DPyP), and the Cr^{3+} ions anchored on other GO sheet can coordinate with the other pyridyl moiety in the 5,15–diphenyl–10,20–di(4–pyridyl) porphyrin (DPyP). That is, the Cr^{3+} ions act as the interfacial linker of the GO and DPyP molecules, and the DPyP pillared GO composite sheets are achieved. It could be profitable to promote the electron transfer between GO sheets and DPyP. Some important interactions are supplied in Scheme S1. Differently, without introduction of the metal ions, there only exists weak π–π interaction between the GO and DPyP. Therefore, the DPyP molecules are flattened onto the surface of the GO in the form of aggregates, just like the images shown in Fig. 1a–1b. The suggested Scheme can be further demonstrated by the following results (XRD, XPS and nitrogen adsorption–desorption isotherms).

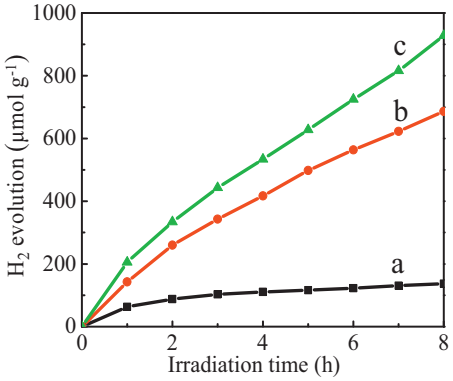

Fig. 7. Time course of photocatalytic hydrogen evolution over various photocatalysts. (a) GO, (b) GO–DPyP composite and (c) GO—Cr^{3+}–DPyP composite using triethanolamine (TEA) as the sacrificial agent under visible irradiation. Reaction conditions: $m_{catalyst}$ = 10 mg, TEA = 10 vol.%, T = 298 K.

To clarify the component of the composite and the distribution of the RGO, DPyP and Cr^{3+}, energy–filtered TEM of the GO—Cr^{3+}–DPyP nanocomposite is taken. Fig. 2 shows the element maps of the as–prepared GO—Cr^{3+}–DPyP nanocomposite. It can be found that there exist C, O, N and Cr elements in the nanocomposite. C element is originated from GO and DPyP. O element and N element come from GO and DPyP, respectively. The density of C element is higher than that of the O element. It is due to the high content of C element in the composite. It is found that the distribution of N element is basically consistent with that of Cr element. Moreover, Cr element is mainly distributed around O element, and the density of N element is higher around Cr element. It demonstrates that DPyP molecules are well dispersed in the composite with the help of Cr^{3+}.

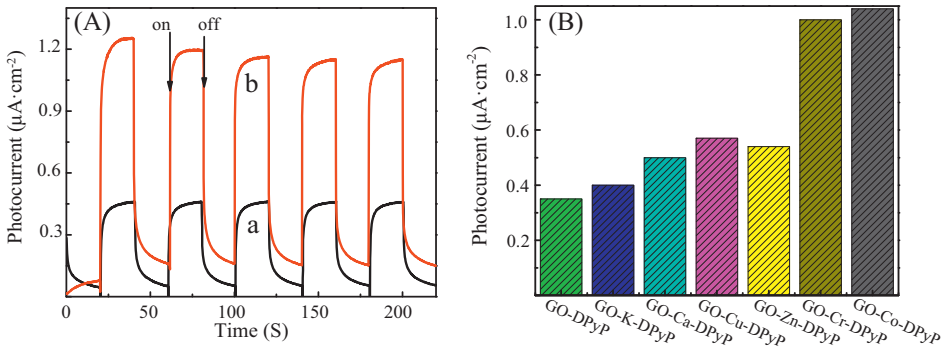

Fig. 8. (A) Photocurrent responses of the FTO electrodes coated with (a) GO–DPyP and (b) GO—Cr^{3+}–DPyP composites; (B) Photocurrent responses of the FTO electrodes coated with GO–DPyP and GO–M–DPyP composites (M = K^+, Ca^{2+}, Cu^{2+}, Zn^{2+}, Cr^{3+}, Co^{2+}), respectively. Supporting electrolyte: 0.5 mol L^{-1} Na_2SO_4 aqueous solution.

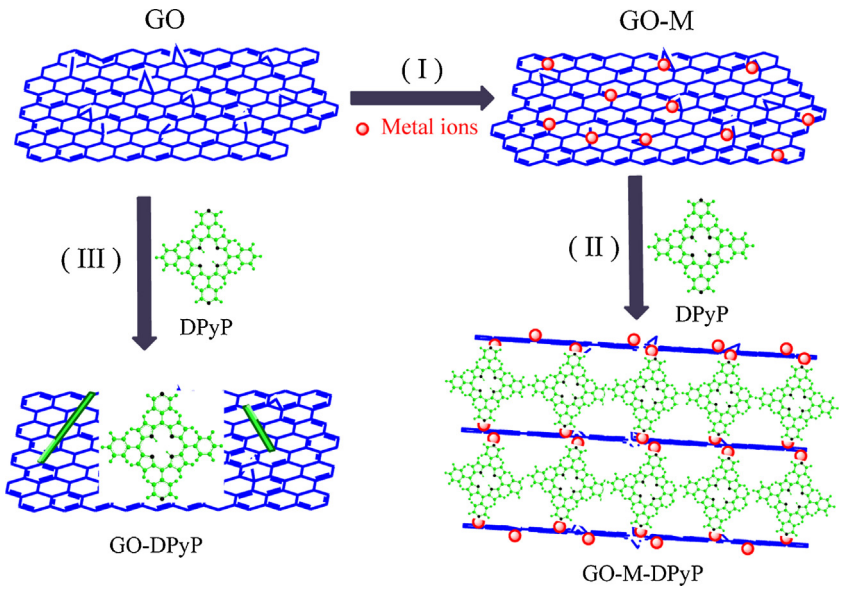

Scheme 2. Suggested formation schemes for the GO–DPyP and the GO–M–DPyP composites. (The drawings are not to scale).

3.2. FTIR spectra

The formation of Cr^{3+} bridged GO–DPyP composites also can be confirmed by FTIR spectra. As shown in Fig. 3b and 3c, the vibrations of carboxylic species, hydroxyl species and epoxy species (C=O stretching, 1738 cm^{-1}; OH deformation, 1400 cm^{-1}; C—OH stretching, 1224 cm^{-1}; C—O—C (epoxy group) stretching, 1066 cm^{-1}; skeletal ring stretching, 1622 cm^{-1}) are consistent with the characteristic vibrations of the GO [28]. No obvious peaks corresponding to DPyP are observed, which is probably attributed to the low content of DPyP in the composite (Approx. 4 wt.%). The presence of DPyP in the composites can be confirmed by solid diffuse reflectance UV–vis absorbance spectra (Fig. S2). A shoulder at 1591 cm^{-1} (Fig. 3c) and the downshift of the C=O vibration from 1738 to 1711 cm^{-1} indicate the coordination of DPyP with Cr^{3+} [29]. As shown in Fig. S3, some absorption bands appear in the fingerprint region of the GO—Cr^{3+}–DPyP composite, and the band near 420 cm^{-1} corresponds to the Cr^{3+}–O bond. Based on the above results, it is deduced that there exists strong interaction between the Cr^{3+} ions and the O atoms on the surface of GO 16. Therefore, the GO—Cr^{3+}–DPyP shows higher thermal stability (Fig. S4).

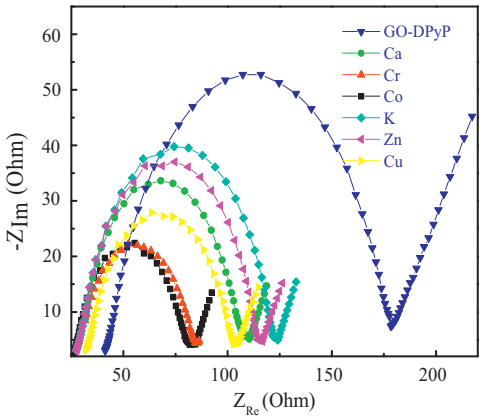

Fig. 9. Nyquist plots of electrochemical impedance spectroscopy for GO–DPyP and GO–M–DPyP nanocomposites (M = K^+, Ca^{2+}, Cu^{2+}, Zn^{2+}, Co^{2+} and Cr^{3+}) in 0.1 mol L^{-1} KCl aqueous solution containing 0.01 mol L^{-1} $K_3Fe(CN)_6/K_4Fe(CN)_6$ (1:1).

It is deduced that metal ions can fix some labile oxygen functional groups in the GO sheets and prohibit them from decomposing.

3.3. X–ray photoelectron spectroscopy

The surface element composition and the valence state of Cr in the GO—Cr–DPyP composite are confirmed by X–ray photoelectron spectroscopy (XPS). The element composition shown in Fig. 4a is consistent with that in Fig. 2. The content of O in the composite is about 60%, which is beneficial for absorbing metal ions. The XPS spectrum of C1s shows the characteristic peaks of C—C/C=C (284.5 eV), C—O—H/C—O—C (286.6 eV) and C=O (288.4 eV), which indicate the presence of epoxide, hydroxyl and carboxyl groups in the composite [30]. In Fig. 4c, the peaks at 589.6 eV, 586.5 eV, 579.2 eV and 576.8 eV are attributed to the $Cr2p_{1/2sat}$, $Cr2p_{1/2}$, $Cr2p_{3/2sat}$ and $Cr2p_{3/2}$, respectively. It indicates the presence of Cr^{3+} ions in the composite. Referenced to the literature [31], the peak at 581.7 eV is attributed to Cr–N.

In the XPS spectrum of N1s (Fig. 4d), four peaks are observed: the peak at 397.9 eV is attributed to the C=N of pyrrole, the peak at 399.4 eV corresponds to the NH of pyrrole, the peak at 401.2 eV is the N of pyridyl (in DPyP) coordinated with Cr^{3+}, and the peak at 398.4 eV is attributed to the N of uncoordinated pyridyl (in DPyP) [32]. These results confirm the formation of the Cr^{3+} bridged GO–DPyP composite.

3.4. Nitrogen adsorption–desorption characteristic of the composites

To reveal adsorption–desorption behaviour and structural change after implanting metal ions in the composite, the nitrogen adsorption–desorption isotherms of the GO, GO–DPyP and the GO—Cr^{3+}–DPyP composites are measured. The isotherm of GO shows a normal type II absorption (Fig. S5). It is indicated that there does not exist pores except random layer stacking of GO sheets [33,34]. As shown in Fig. 5, the isotherm of GO–DPyP composite shows a normal type III absorption with a type H3 hysteresis loop at higher relative pressure, while the isotherm of GO–M–DPyP composite displays a normal type III absorption with a type H4 hysteresis loop at higher relative pressure. It is known that type H3 hysteresis loop corresponds to the slit pores. While the type H4 hysteresis loop is inclined to layer by layer stacking

[35]. The GO–M–DPyP exhibits a microporous structure (Fig. S6). Adsorption average pore width is about 6 nm. The size distribution of the porous is wide maybe due to the random coordination between metal ions on the GO–M and pyridyl moieties in the 5,15–diphenyl–10,20–di(4–pyridyl) porphyrin (DPyP). The result is consistent with those in Fig. 1 and Scheme 2. The BET surface areas of the GO, the GO–DPyP composite and the GO–M–DPyP composite are 804.6 $m^2 g^{-1}$, 60 $m^2 g^{-1}$ and 39 $m^2 g^{-1}$, respectively. The decreased surface area may be due to enfoldment and rearrangement of the GO sheets after introducing metal ions and DPyP.

3.5. XRD analysis

Furthermore, the structures of the samples are characterized by XRD. As shown in Fig. 6a, the peak at 10.3° is attributed to the (001) face of the GO, and it corresponds to an interlayer space of 8.6 Å. For the GO–DPyP and GO – Cr^{3+} composites, the peaks are located at the same position as the pure GO (Fig. 6b and Fig. 6c). After introducing DPyP in the GO – Cr^{3+} composites, the peak is shifted to 9° (Fig. 6c), corresponding to an interlayer space of 9.8 Å. The enlarged interlayer space shows that the formation of the DPyP pillared GO–DPyP composite with the help of the metal ions. The interlayer space is smaller than the size of the DPyP, which indicates the included angle between DPyP molecule and GO sheets is lower than 90°. The result is consistent with those shown in Fig. 1, Fig. 4 and Fig. 5.

3.6. Photocatalytic hydrogen evolution and interfacial electron transfer

As shown in Fig. 7, without adding any cocatalysts, under visible irradiation for 8 h, the total amount of H_2 evolved over the GO, GO–DPyP and GO—Cr^{3+}–DPyP reach 137, 686, 928 μmol g^{-1}, respectively. GO—Cr^{3+}–DPyP composite shows the highest photocatalytic activity.

In order to know the reason for the enhanced photocatalytic activity in the GO—Cr^{3+}–DPyP composite, it is important to investigate the photoelectron transfer in the composites. It is known that the photocurrent generation can be attributed to photoelectron transfer. Therefore, photocurrent responses and electrochemical impedance spectroscopy of the samples are measured. As shown in Fig. 8, after turning on the light, the photocurrent is quickly enhanced. It is demonstrated that the composites are photosensitive, and photoelectron transfer from DPyP to GO sheets can take place. Compared with that of the GO–DPyP, the photocurrent of the GO—Cr^{3+}–DPyP is drastically enhanced, indicating the positive role of the Cr^{3+} as the interfacial linker.

It is found that, not only Cr^{3+}, many metal ions (such as K^+, Ca^{2+}, Zn^{2+}, Cu^{2+} and Co^{2+}) also have positive influence on the photocurrent response of the GO – DPyP composite (Fig. 8B). It is demonstrated that the implantation of metal ions is able to promote the photoelectron transfer across the interface between DPyP and GO. Therefore, the photocurrent is enhanced. The photocurrent response of the GO – DPyP composite implanted Co^{2+} or Cr^{3+} are higher than the other metal ions. It could be attributed to the stronger coordination interaction between metal ions and DPyP.

Furthermore, the charge carrier migration in the nanocomposite was characterized. As shown in Fig. 9, the diameters of the semicircles at high frequencies for various composites are distinctly different. The diameters of the semicircles become smaller after implanting metal ions. It is indicated that there exist lower interfacial resistance in the GO–M–DPyP electrodes. Subsequently, implanting metal ions in the interface of GO and DPyP can significantly optimize the electron transfer pathway and promote the electron transfer, and thus enhance the photocurrent of the composite electrodes. In addition, fluorescence of the composite is quenched after being implanted metal ions (Fig. S7). It is another evidence for efficient and rapid electron transfer can take place in the GO–M–DPyP composite with the metal ions as the interfacial linker. Combined with the results in Fig. 7–Fig. 9, it is shown that metal ions act as interfacial electron–transfer mediators, and promote photogenerated charge separation by transferring photoelectrons quickly, which is the key to enhance the photocatalytic activity of the GO/DPyP composites.

4. Conclusion

With metal ions as interfacial linkers, a serial of GO–M–DPyP nanocomposites with excellent performance were achieved. It was found that implanting metal ions in the interface of GO and DPyP can modify the morphology and the structure of the GO–DPyP composite. More importantly, the strong interaction between metal ions and DPyP/GO can facilitate the separation of photoproduced electron–hole pairs and promote the electron transfer between GO and DPyP. Therefore, it led to higher photocatalytic activity for hydrogen production. The facile strategy supplies a common way for constructing the GO–based functional composites with enhanced electron transfer.

Acknowledgements

This work was financially supported by the National Natural Science Foundation of China (NSFC) (Grant Nos. 21301118, 21305092, 21371070 and 21071060), and Innovation Program of Shanghai Municipal Education Commission (No. 15ZZ096).

Appendix A. Supplementary data

Supplementary data associated with this article can be found, in the online version, at http://dx.doi.org/10.1016/j.apcatb.2016.01.024.

References

[1] C.L. Yu, J.C. Yu, Catal. Lett. 129 (2009) 462–470.
[2] V. Georgakilas, M. Otyepka, A.B. Bourlinos, V. Chandra, N. Kim, K.C. Kemp, P. Hobza, R. Zboril, K.S. Kim, Chem. Rev. 112 (2012) 6156–6214.
[3] X.J. Wan, Y. Huang, Y.S. Chen, Acc. Chem. Res. 45 (2012) 598–607.
[4] M.Y. Yen, M.C. Hsiao, S.H. Liao, P.I. Liu, H.M. Tsai, C.C.M. Ma, N.W. Pu, M.D. Ger, Carbon 49 (2011) 3597–3606.
[5] X.Q. Zhang, Y.Y. Feng, S.D. Tang, W. Feng, Carbon 48 (2010) 211–216.
[6] C.H. Lu, H.H. Yang, C.L. Zhu, X. Chen, G.N. Chen, Angew. Chem. Int. Ed. 48 (2009) 4785–4787.
[7] Q.Y. He, S.X. Wu, Z.Y. Yin, H. Zhang, Chem. Sci. 3 (2012) 1764–1772.
[8] D.M. Chen, K.W. Wang, W.Z. Hong, R.L. Zong, W.Q. Yao, Y.F. Zhu, Appl. Catal. B: Environ. 166–167 (2015) 366–373.
[9] C. Trinh, M.T. Whited, A. Steiner, C.J. Tassone, M.F. Toney, M.E. Thompson, Chem. Mater. 24 (2012) 2583–2591.
[10] M.S. Zhu, Z. Li, B. Xiao, Y.T. Lu, Y.K. Du, P. Yang, X.M. Wang, ACS Appl. Mater. Interfaces 5 (2013) 1732–1740.
[11] C. Kong, G. Zhang, Y. Li, D.W. Li, Y.T. Long, RSC Adv. 3 (2013) 3503–3507.
[12] H. Hayashi, I.V. Lightcap, M. Tsujimoto, M. Takano, T. Umeyama, P.V. Kamat, H. Imahori, J. Am. Chem. Soc. 133 (2011) 7684–7687.
[13] L.Q. Jiang, M. Li, L. Lin, Y.F. Li, X.Q. He, L.L. Cui, RSC Adv. 4 (2014) 26653–26661.
[14] Y.X. Xu, L. Zhao, H. Bai, W.J. Hong, C. Li, G.Q. Shi, J. Am. Chem. Soc. 131 (2009) 13490–13497.
[15] B. Qiu, M. Xing, J. Zhang, J. Mater. Chem. A 3 (2015) 12820–12827.
[16] B. Qiu, Y. Zhou, Y. Ma, X. Yang, W. Sheng, M. Xing, J. Zhang, Sci. Rep. 5 (2015) 8591–8596.
[17] S. Li, D.Q. Wu, C. Cheng, J.Z. Wang, F. Zhang, Y.Z. Su, X.L. Feng, Angew. Chem. Int. Ed. 125 (2013) 12327–12331.
[18] B.C. Qiu, M.Y. Xing, J.L. Zhang, J. Am. Chem. Soc. 136 (2014) 5852–5855.
[19] Y.S. Huang, D.Q. Wu, J.Z. Wang, S. Han, L. Lv, F. Zhang, X.L. Feng, Small 10 (2014) 2226–2232.
[20] N. Zhang, M.Q. Yang, Z.R. Tang, Y.J. Xu, ACS Nano 8 (2014) 623–633.
[21] H.P. Cong, P. Wang, S.H. Yu, Small 10 (2014) 448–453.
[22] E. Alessio, M. Casanova, E. Zangrando, E. Lengo, Chem. Commun. 48 (2012) 5112–5114.
[23] A. Kira, T. Umeyama, Y. Matano, K. Yoshida, S. Isoda, J.K. Park, D. Kim, H. Imahori, J. Am. Chem. Soc. 131 (2009) 3198–3200.

[24] N.I. Kovtyukhova, P.J. Ollivier, B.R. Martin, T.E. Mallouk, S.A. Chizhik, E.V. Buzaneva, A.D. Gorchinskiy, Chem. Mater. 11 (1999) 771–778.
[25] W.S. Hummers, R.E. Offeman, J. Am. Chem. Soc. 80 (1958) 1339.
[26] P.P. Guo, P.L. Chen, M.H. Liu, ACS Appl. Mater. Interfaces 5 (2013) 5336–5345.
[27] Y. Huang, D. Wu, S. Han, S. Li, L. Xiao, F. Zhang, X. Feng, ChemSus-Chem. 6 (2013) 1510–1515.
[28] J.W. Liu, Y. Zhang, X.W. Chen, J.H. Wang, ACS Appl. Mater. Interfaces 6 (2014) 10196–10204.
[29] S. Bettini, R. Pagano, L. Valli, G. Giancane, J. Phys. Chem. C 118 (2014) 12384–12390.
[30] X.J. Liu, L.Y. Cao, W. Song, K.L. Ai, L.H. Lu, ACS Appl. Mater. Interfaces 3 (2011) 2944–2952.
[31] K. Artyushkova, C. Walker, W. Patterson, P. Atanassov, Electrocatalysis 5 (2014) 241–247.
[32] J.R. Eskelsen, Y. Qi, S. Schneider-Pollack, S. Schmitt, K.W. Hipps, U. Mazur, Nanoscale 6 (2014) 316–327.
[33] C. Tien, Adsorption calculation and modeling, in: Series in Chemical Engineering, Butterworth-Heinemann, London, 1994.
[34] M. Kruk, M. Jaroniec, Chem. Mater. 13 (2001) 3169–3183.
[35] G. Moon, Y. Shin, D. Choi, B.W. Arey, G.J. Exarhos, C.M. Wang, W. Choi, J. Liu, Nanoscale 5 (2013) 6291–6296.